



Sustainable Solutions for Energy and Environment, EENVIRO 2016, 26-28 October 2016,
Bucharest, Romania

Numerical simulation of non-normal wind load on porous fences

Yizhong Xu^{a,*}, Mohamad Y^a. Mustafa, Rajnish K. Calay^a, Bjørn S. Sørensen^a

^a*UiT/the Arctic University of Norway, Narvik, 8515, Norway*

Abstract

This paper presents a numerical simulation of non-normal wind loads on a porous fence. It was found that non-normal wind load has significant impact on the performance of the fence in terms. The performance of the fence was measured as the effective fence zone behind the fence where flow characteristics and normal drag coefficients were maintained within safe level. It is recommended the incidental angle between the most prevalent wind direction and the fence position is preferably less than 15° but and no more than 30°.

© 2017 The Authors. Published by Elsevier Ltd. This is an open access article under the CC BY-NC-ND license (<http://creativecommons.org/licenses/by-nc-nd/4.0/>).

Peer-review under responsibility of the organizing committee of the international conference on Sustainable Solutions for Energy and Environment 2016

Keywords: porous fence; non-normal wind load; CFD; effective fence zone; drag coefficient;

1. Introduction

Porous fences are commonly designed with openings of certain shape, size and distribution in the form of windbreaks enabling natural climate under control. In real applications, it is not realistic to expect that such fences encounter wind flow in the normal direction at all times. In fact, natural wind keeps changing its direction with time; consequently, the wind load on a fence also changes dynamically. However, for a designated location, statistically natural wind comes a certain degree of directions more often than the other directions. This suggests that allocating fences in a specific area should take considerations of such statistic degree of wind directions to maximize their performance.

* Corresponding author. Tel.: +47 769 6 6544.
E-mail address: Yizhong.xu@uit.no

Wind load on a solid panel are relatively simple and can be written as the following:

$$F = 0.5c_d A_{ref} \rho U_{ref}^2 \quad (1)$$

where: c_d is the aerodynamic force coefficient (or drag coefficient) dependent on the shape and the material of the panel. For porous fences, the porous effects on wind load can be significant, which may be considered in a modified c_d . Richards & Robinson [1] found that the loss coefficient is a function of porosity and the construction of the fence. They proposed a concept of the effective porosity β_e defined as the porosity of a round-wire meshed screen with the same loss coefficient, and suggested that wind loads on porous structures were reduced by a factor of $(1 - \beta_e)$ if compared with those of solid structures. Letchford [2] performed the wind tunnel experiments to investigate c_d for elevated permeable and impermeable panels, where the dependence of c_d on the geometric characteristics of height, width and bottom gap have been studied. He proposed a correction factor for the low porous panel, which was $1 - \beta^{1/2}$. It must be noted that his study was focused on elevated impermeable and low porosity (less than 0.23) panels.

When a porous fence encounters non-normal wind flow incident at an angle θ , where θ is the angle between the wind direction and a perpendicular to the fence, it is obvious that the effective area of the fence is reduced by a factor of $\cos \theta$. The acting wind at the angle would also have air motions parallel to the fence panel, thus the normal force component causes pressure and the force component paralleled to the panel induces shear or frictional drag.

In this paper, the effect of non-normal wind loads on the performance of a porous fence was numerically investigated using computational fluid dynamics (CFD) techniques. Numerical simulations were performed with a commercial code ANSYS FLUENT 14.0 Research version. The information of the flow characteristics around the fence as well as the structure of the velocity distribution on the fence were obtained, then the forces on the fence were calculated, which provides useful information to study the stability and structural integrity of the fence. The effective fence zone, which is another key performance parameter of the fence, was also obtained and estimated.

Nomenclature

F	force on the panel
c_d	drag coefficient
A_{ref}	reference area
ρ	density of air
U_{ref}	wind velocity at a reference height
β	porosity
β_e	effective porosity
θ	angle of non-normal wind load
CFD	computational fluid dynamics
H	fence height
L1	effective shelter distance
h1	height of crest

2. Development of the numerical Model

Test panel: The size of the test fence panel used in this study was 400mm wide, 200mm high and 3mm thick. Usually porous fences have circle or oval shaped pores. The testing fence was designed to have uniformly distributed circular shaped pores with the diameter of 50mm, which provides the porosity value of 0.3. It is within the recommended range of porosity to optimize the performance of porous wind fences, where porosity value between 0.3 and 0.4 leads to greatest wind reduction over a longer distance on the leeward side [3], [4] [5].

Computational Domain and boundary conditions: Ideally numerical domain is better to have a large size enough to eliminate the effects of boundaries. The size of the testing domain was 8.0m long, 2.4m wide and 1.2m high, and the fence was placed at the center of the cross section in the domain at a longitudinal distance of 3m from the inlet,

which is 15 times of the fence height. The distance between the fence side edge and the domain sidewall was 1.0m, which is 5 times of the fence height. This configuration ensured that the effects of boundaries are minimal.

The inlet velocity profile was set as uniform at 10m/s and the outlet was set as zero Gauge pressure. The turbulence intensity and turbulent viscosity for inlet and outlet were both set as 5%. The turbulence model was two-equation based Standard $k-\epsilon$ model. The boundary walls were treated as no-slip walls. Six test cases to simulate the effect of wind on the fence coming from different angles. Incident angles θ was changed from 0° , 10° , 15° , 30° , 45° and 60° .

Fig. 1 displays the mesh detail near the fence and the ground. In order to capture the sharp gradients in the flow within the boundary layer around the test section and near the ground region, mesh elements were made using triangular prism grid highlighted in the red frame in Fig. 1. In other regions tetrahedron elements. Several grid sizes were tested to obtain grid independent results. The grid size with around 0.85 million elements was found the grid independence.

Further detail about numerical procedure and validation of the model are presented in another paper [6].

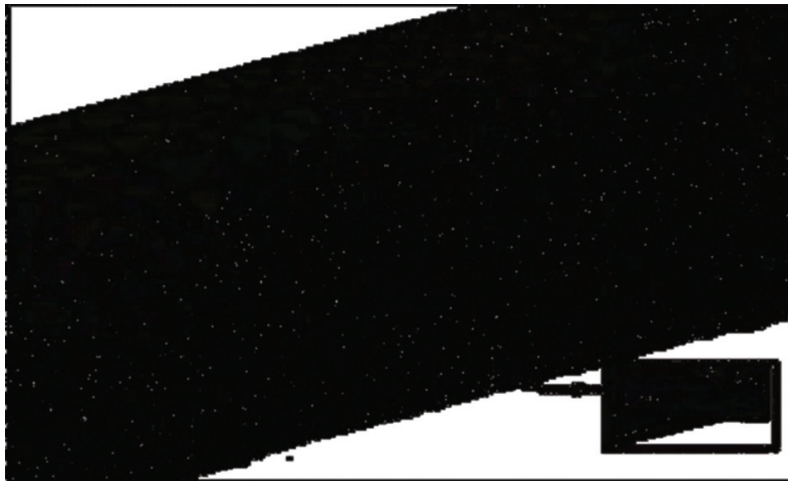


Fig. 1: The detailed mesh in the near fence and the ground for the 3D model

3. Results and discussions

3.1. Effective fence zone

The definition of the effective fence zone (or the fence protection zone) is vague in fence applications. Raine & Stevenson [7] suggested that such zone should give a mean wind velocity reduction of 50% up to $10H$ downstream, 20% up to $20H$ downstream, and a maximum reduction of 70-80% between $1H$ and $5H$ downstream. These values were measured at half of fence height.

In this study, the effective fence zone was assessed by 40% of mean velocity reduction i.e. where velocity values were less than or equal to $6m/s$. For comparisons, the reference plane was selected as the YZ plane at the centre of the longitudinal cross section.

Fig. 2 shows the effective fence zones at different angles of wind load. The size of the effective fence zone is measured by the shelter distance of Ll and the height of the crest of hl . It is observed that non-normal wind load influenced its size. As the angle θ increased, the size was reduced. Increasing the angle θ from 0° to 10° , it caused the shelter distance to be shortened to about 30%. Further decrease in the angle θ i.e. 10° to 30° , decrease in the shelter distance is gentle, however, after 30° , the shelter distance decreases dramatically.

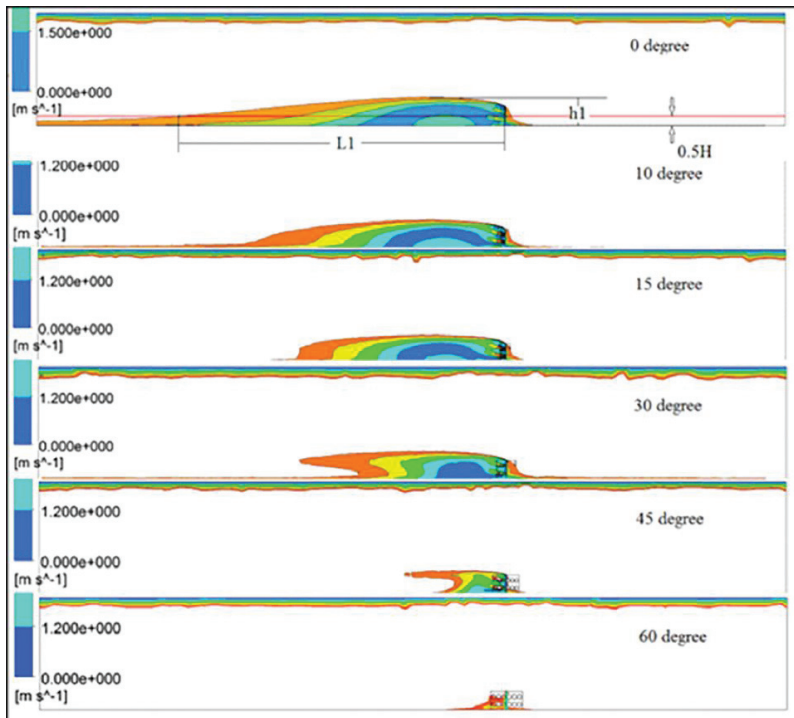


Fig.2: The effective fence zones at different angles of wind load

Further investigation on the effective fence zone was performed to offset plane-1 to $x/H = 0.25, 0.5$ and 0.75 , respectively. The variation of shelter distance expressed as a dimensionless distance $L1/H$ with respect to change in the incidence angel at different x positions is shown in Fig. 3.

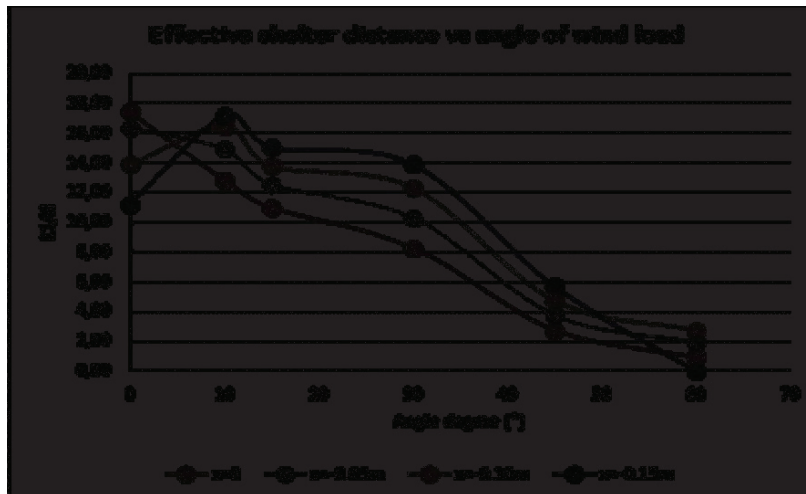


Fig. 3: The dimensionless effective shelter distance vs angle of wind load for the plane-1 at different x positions

Fig. 4 shows the variation of dimensionless height crest expressed as $h1/H$ with respect to change in the incidence angle at different x positions. Fig. 5 shows the flow streamlines at different angles.

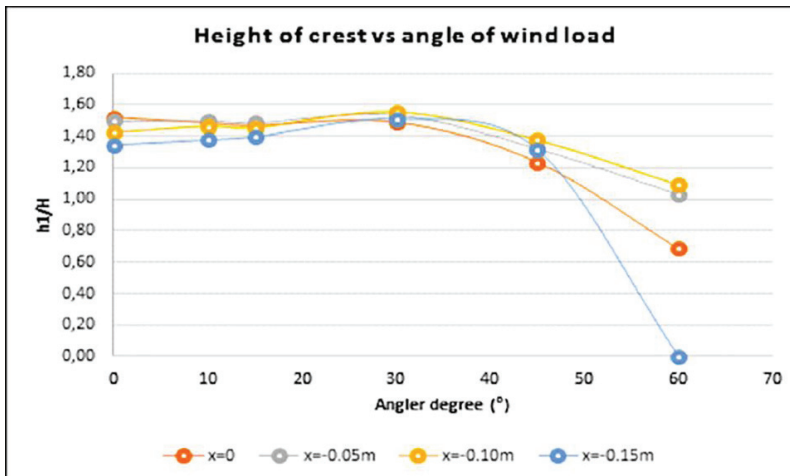


Fig. 4: The dimensionless height crest vs angle degree for the plane-1 at different x positions

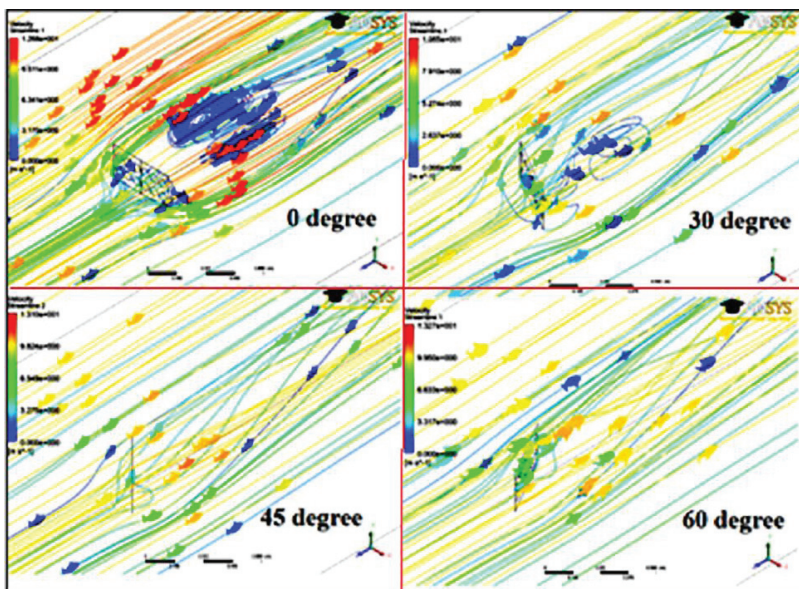


Fig. 5: Streamlines around the fence at different angles of wind load

It is evident from the above figures that the effective shelter distance decreases as the angle increases. However, the effective shelter distance appears to increase for angles between 0° and 10° , and the regions between $x = -0.10m$ and $x = -0.15m$. The maximum effective shelter distance is at $x = 0m$ with $\theta = 0$, i.e. when wind approaches normal to the fence surface.

Both of Fig.3 & Fig. 4 also revealed that the effective shelter distance dropped relatively slowly in the range from 10° to 30° . It was found that the height of crest was almost stable in this region shown in Fig.4. This can be

attributed to the fact that the height of crest was more associated with the fence height in the fence effective region. The results revealed that when wind approaches the fence at an angle greater than 45°, it almost destroyed the entire effective fence zone. Therefore, the fence should be placed at a degree of angle no more than 30° to the prevailing wind directions. Preferably, it is recommended to place the fence at an angle less than 15°.

Since angle θ has effects in the area of normal fence and normal wind force, it is possible to describe the effective shelter distance as a function of $\cos^2 \theta$. Fig. 6 shows a linearized correlation between effective shelter distance ($L1/H$) and $\cos^2 \theta$. The effective shelter distance can be estimated as the following:

$$L1/H = a \cos^2 \theta + b \tag{2}$$

where, a and b are empirical constants. In this case, it was found to be between 17.50 and 19.50 for a , and between 2.30 and 5.50 for b , respectively.

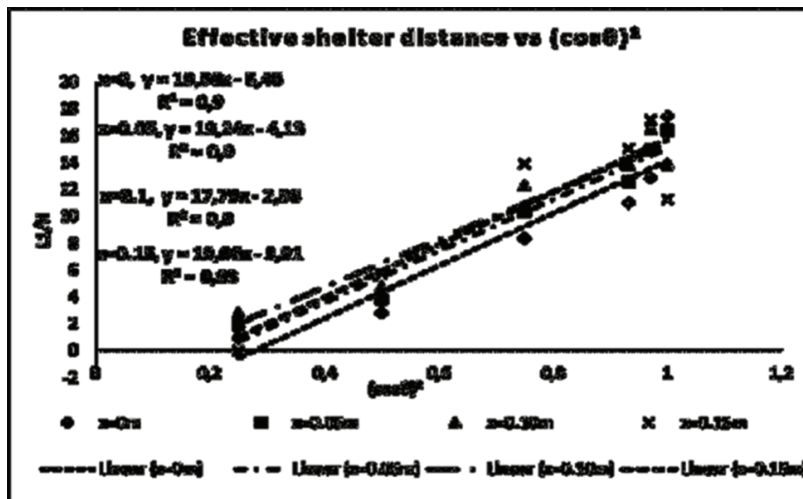


Fig. 6: Linearized effective shelter distance vs $\cos^2 \theta$

The R-squared value of R^2 displayed in Fig.6 is the coefficient of multiple determinations for multiple regressions that the values are around 0.9, which indicates that the linearized correlation explains all the variability of the response data close to its mean. Hence, the linearized correlation may be used as a simplified estimation to predict the effect of the angle θ on the effective shelter distance, although the data in Fig.6 are in fact scattered.

3.2. Load forces and drag coefficient

The wind-induced forces on the fence can be classified as two sources. One is pressure force acting normal to the fence, and another is viscous or shear force acting parallel to the surface due to the fluid viscosity, which is proportional to the vertical velocity gradient. The contribution to the viscous forces in the present case was neglected. Therefore, the following discussions will not take the effect of viscous forces.

Table 1 lists the three dimensional force vectors and the drag coefficients vs. different angles of wind load on the fence. As the angles of wind load increases, x-axial force component also increased. At the angle of 60°, the value of the x-axial force component was greater than the value of the z-axial force component. Due to the variation of the angles of wind load in the XZ-plane, the y-axial force component was created by the circular edges of pores that is small compared to x- and z- axial components thus can be neglected.

The values of the z-axial force component and the drag coefficient decreased with increasing angles except in the range between 30° and 45° . In the range between 0° and 15° , the z-axial force component and the drag coefficient appeared relatively stable, while at the angle of 60° , both of them have been reduced to a significantly small value. Such phenomenon was similar to the findings in the investigation of effective fence zone. It indicates that when the angle was less or equal to 15° , the structure of the flow regime would not be affected noticeably

Table 1: Load force components and drag coefficients at different angles of wind load

Item	Force (N)			Normal drag coefficient
	X-	Y-	Z-	
0°	0.12	0.07	5.40	2.80
10°	0.88	0.07	5.09	2.73
15°	1.28	0.08	4.90	2.51
30°	1.55	0.05	2.79	2.01
45°	3.11	0.08	3.28	2.12
60°	3.17	0.07	1.96	1.15

Fig. 7 shows the comparison of the drag coefficients predicted by the numerical simulations and by the calculations with the drag coefficient at 0° multiplied with a factor of $\cos^2 \theta$, i.e. $2.8 * \cos^2 \theta$.

Good agreement between the values obtained by simulation and empirical relationship was found between angle 0° and 30° , which was compatible to the finding of the other researchers [1]. However, beyond 30° , drag coefficient

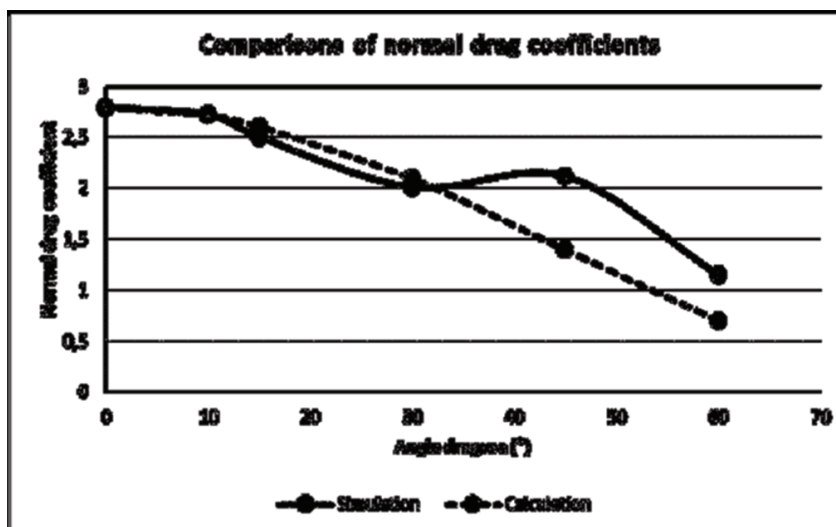


Fig. 7: Comparisons of normal drag coefficients by simulations and calculations

predicted by the simulations increases up to 45° , thus the normal drag coefficients were unlikely to be predicted by a factor of $\cos^2 \theta$.

It must also be mentioned that normal drag coefficient values as obtained by the numerical simulations were higher than the ones from some physical experiments [1] [2] [8]. One reason is that the results obtained by physical tests were for the fences used for different application and have different porosity and different configurations (i.e. Letchford's investigation on signboards and hoardings [2]). Since drag coefficient is always associated with a particular surface area, a particular fence with a porosity of 0.3 creates a structure of flow regime leeward the fence, which is usually more complex than the fence with lower porosity or higher porosity.

4. Conclusions

The numerical investigations presented in this paper discussed the effect of non-normal wind loads on the porous fence through analyzing the effective fence zone, the structure of velocity streamlines, force components and drag coefficient. It was found that the fence should be placed within the angle of $\theta \leq 30^\circ$ to the prevailing wind direction where the effective shelter distance can be estimated in a linearized manner, and the normal drag coefficient could be described as a function of $\cos^2 \theta$. Beyond this angle, shelter distance varies non-linear fashion and its fence performance sharply deteriorates. To maintain the effectiveness of the fence, it is recommended that the fence should be positioned at preferably within 15° angle but never more than 30° angle to the prevailing wind direction.

Acknowledgements

Norwegian Research Council financed this work under project number 195153 (ColdTech). The authors would also like to acknowledge the support from the Arctic University of Norway and colleagues.

References

- [1] Richards, P.; Robinson, M., "Wind loads on porous structures," *Wind Engineering and Industrial Aerodynamics*, pp. 455-465, 1999.
- [2] C. Letchford, "Wind loads on rectangular signboards and hoardings," *Wind Engineering and Industrial Aerodynamics*, pp. 135-151, 2001.
- [3] B. Blocken, "50 years of computational wind engineering: past, present and future," *Wind Engineering and Industrial Aerodynamics*, pp. 69-102, 2014.
- [4] Bourdin, P.; Wilson, J., "Windbreak aerodynamics: is computational fluid dynamics reliable?," *Boundary-Layer Meteorology*, pp. 181-208, 2008.
- [5] A. Packwood, "Flow through porous fences in thick boundary layers: comparisons between laboratory and numerical experiments," *Wind Engineering and Industrial Aerodynamics*, pp. 75-90, 2000.
- [6] Xu, Yizhong; Mustafa, Mohamad Y., "Investigation of the structure of airflow behind a porous fence aided by CFD based virtual sensor data," *Sensors & Transducers*, pp. 149-155, 2015.
- [7] Raine, J.; Stevenson, D., "Wind protection by model fences in simulated atmospheric boundary layer," *Wind Engineering and Industrial Aerodynamics*, pp. 159-180, 1977.
- [8] L. Hagen and E. Skidmore, "Turbulent velocity fluctuations and vertical flow as affected by windbreak porosity," *Trans ASAE*, pp. 634-637, 1971.